



Research Article

Linearized layering method for stress intensity factor determination



Bradley Storm¹  · Jeries J. Abou-Hanna¹

Received: 31 May 2022 / Accepted: 11 November 2022

Published online: 08 December 2022

© The Author(s) 2022 **OPEN**

Abstract

This paper looks to reduce the complexity of determining stress intensity factors while maintaining high levels of accuracy by the use of a linearized layering approach. Many techniques for stress intensity factor determination exist, but they can be limited by conservative results, requiring too many user parameters, or by being too computationally intensive. Multiple notch geometries with various crack lengths were investigated in this study to better understand the effectiveness of the proposed method. By linearizing the average stresses in radial layers around the crack opening, stress intensity factors were found to have error ranging from -10.03 to 8.94% when compared to analytically exact solutions. This approach proved to be a robust and efficient method of accurately determining stress intensity factors.

Article highlights

- An approach to determine stress intensity factors by linearizing a layered notch stress profile is presented.
- Stress intensity factors for multiple notch geometries are investigated and tested using the Linearized Layering Method.
- The Linearized Layering Method is a robust and effective method to determine stress intensity factors.

Keywords Fracture mechanics · Finite element method · Stress intensity factor · Stress linearization

1 Introduction

The stress intensity factor is one of the most fundamental and useful parameters in fracture mechanics and is used to describe the stress state near the tip of a crack caused by remote loading or residual stresses. Current methods can be limiting because they are overly conservative, require too many user parameters, or can be very computationally intensive, such as the finite element-based techniques that can also produce divergent solutions. The purpose of this work is to establish a simple and robust

method of determining stress intensity factors for linear elastic fracture mechanics analysis. This study is based on the understanding that a single maximum stress value approach cannot accurately explain fracture from stress concentration locations, but instead a critical volume in which the crack resides must be considered. Overall, this work aims to provide the practicing engineer a robust and accurate way to calculate stress intensity factors. In the next section, the literary background for the study is discussed, in Sect. 3 the proposed methodology is discussed in detail, Sect. 4 shows the case studies' results, and in the

✉ Bradley Storm, bstorm@mail.bradley.edu | ¹Department of Mechanical Engineering, Bradley University, Peoria, IL 61625, USA.



last section, final observations and conclusions about the method are made.

2 Literature background

The approach derives from the following founding equation for stress intensity developed by Irwin [1],

$$K = F\sigma\sqrt{\pi a}, \quad (1)$$

where F is used to represent various correction factors indicated in studies and works like Murakami's [2]. It has also been shown by Murakami [3] and Murakami and Endo [4, 5] that the stress intensity factor can be determined as a function of square root of crack area to a 10% degree of accuracy. Glinka [6] performed modifications to Eq. 1, replacing the crack length, a , with a term characterizing a notch-tip radius. Bloom and Van Der Sluys [7] utilized methods considering the stresses along the length of the crack to determine stress intensity factors. Chen [8] introduced the use of a body force method to find stress intensity factors for a strip plate with single or double edge notches under tension or in-plane bending. Furthermore, Liu et al. [9] implemented the use of numerical methods and the finite element method to determine multiple stress singularities and related stress intensity factors. Chell [10, 11] proposed that the stress-intensity factor for an arbitrarily loaded crack could be given as the product of a compliance function for the crack subjected to a uniform stress and a weighted integral involving the arbitrary stress. A weight function method for determining stress-intensity factors was developed by Bueckner [12] and Rice [13]. Ju and Chung [14] used the finite element method and a least squares method to find 3D stress intensity factors of a sharp v-notch. Xu et al. [15] proposed a numerical method that doesn't need the asymptotic solution of the singular stress field to determine the orders of the multiple stress singularities and related stress intensity factors. Courtin [16] showed the advantages of using the J-integral approach [17] in stress intensity factor determination. The J-integral technique has been expanded upon by those such as Gopichand [18], Nikolova [19], Azmi [20] and Han [21], proving it has good accuracy and effectiveness. Alatawi [22] showed another alternative method, the extended dual boundary element method, providing the value for stress intensity factor directly in the solution vector and without the need for postprocessing. Gupta [23] investigated and compared three different methods for determining stress intensity factor: the Cutoff Function Method, the Contour Integral Method, and the Displacement Correlation Method, showing the advantages of the Displacement Correlation Method in determining stress

intensity factors when using domain integrals is not possible. Farahani [24] developed a radial point interpolation meshless method that calculated stress intensity factors with good accuracy. Determination of stress intensity factors through digital image correlation has also been studied by those such as Roux [25], Gonzales [26] and Tavares [27]. Berto [28] calculated mixed mode stress intensity factors of V-notches using refined FE meshes. This paper utilizes similar methods in using superposition and FEA to calculate stress intensity factors. Linearized stress distributions to find stress intensity factors were used by Dong [29] and compared to those determined by finite element method. A combination of a weighting function and radial layering were implemented by McKinley [30] and Abou-Hanna [31] to determine stress intensity factors within a $\pm 10\%$ error band. Use of the radial layering approach showed great promise and is expanded upon in this study.

3 Proposed methodology

Utilizing FEA on a 2-D rectangular plate, crack free linear-elastic specimens were used in determining Mode I stress intensity factors. The principal stress, σ_y , was used throughout this study because it is the stress perpendicular to the crack. The cartesian coordinate system was used for all 2-D cases. The approach begins with dividing the area around the crack opening into radial layers emanating at the crack opening. This approach can also be applied to a 3-D case, using spherical layers instead. A representation of the radial stress layering for a notched component is shown in

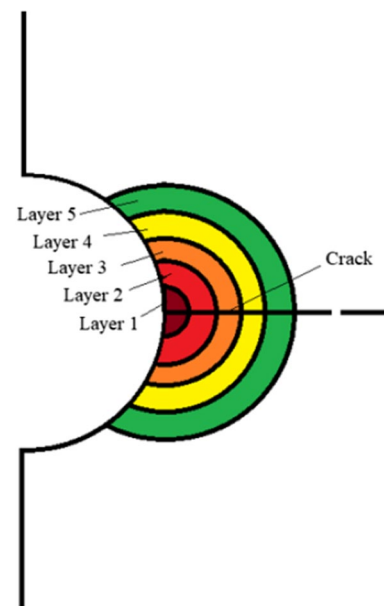


Fig. 1 Radial layering for a notched component

Fig. 1. The stress values within each layer are averaged and used to create a 1-D stress profile that represents stress vs. radial distance from the component surface. This stress profile can be linearized, and the resulting membrane and bending stresses extracted. The membrane stress is the average of the linearized curve, and the bending stress is the difference between the maximum value of the linearized curve and the average. Figure 2 shows how the nonlinear stress profile from Fig. 1 would look like and also what the linearization with membrane and bending stresses would look like.

Determination of how much of the stress profile to linearize is governed by the consideration that a critical area of material exists where the crack resides. Deciding how much of the stress profile to linearize is one of the main investigations of this work. The distance at which the stress will be linearized from the crack opening will be referred to as the “linearization range” (LR). The LRs used in this investigation were dependent on the size of the crack, varying from 1× the crack length to 7× the crack length. The membrane stress and bending stress can be extracted from the linearized stress curve and used separately in stress intensity factor calculations. Dowling [32] showed that stress intensity solutions for combined loading can be obtained by summing each individual load components’ corresponding stress intensity factors. This linear superposition is the main assumption in this study hypothesizing that the total mode I stress intensity factor is the sum of the bending and membrane stress induced intensities. This is the basis of the hypothesis of this proposed approach:

$$K_b = \sigma_b \sqrt{\pi a} \quad (2)$$

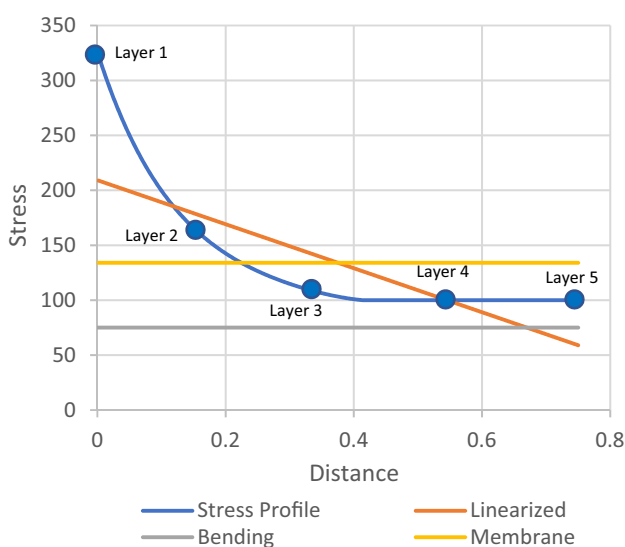


Fig. 2 Nonlinear stress profile and linearization

$$K_m = \sigma_m \sqrt{\pi a} \quad (3)$$

where K_b is the stress intensity factor from the bending stress σ_b , K_m is the stress intensity factor from the membrane stress σ_m , and a is the length of the crack. The total stress intensity factor can then be found by summing the stress intensity factors from the bending and membrane stresses:

$$K = K_b + K_m. \quad (4)$$

The proposed method was investigated by comparing stress intensity factors of differing LRs with those readily available in engineering handbooks. Three separate cases were explored to help determine effectiveness of the method. The finite element analysis of this study was conducted using ABAQUS FEA.

A state of plane strain was assumed for cases 4.1 and 4.2 involving the 2-D plate.

4 Case studies

4.1 A crack emanating from a round center hole in a plate under uniaxial tension

Center holes of diameters 25% and 50% of the width of the plate were used, while the height of the plate was twice that of the width in order to ensure far field load conditions. A quarter symmetry mesh model with a notch 0.25 that of the width is shown in Fig. 3. A 100 MPa pressure was applied uniformly to the top edge of the model. The properties of the material represent alloy steel with a modulus of elasticity of 205 GPa and a Poisson’s ratio of 0.29. Symmetrical boundary conditions were applied such that the nodes on the bottom and right edge of the model have their displacement components normal to their respective planes constrained. The radial layers within the model were created to have layers closer together near the crack opening where the stress gradient is the highest, and layers farther apart where the stress gradient is smaller. Figure 4 shows the radial layers created in the model. A thickness of at least 3 elements between each layer was used to ensure accuracy of the mesh.

A mesh sensitivity analysis was conducted to determine the optimum element size. Figure 5 compares the stress calculated when increasing the number of elements used as the thickness of the radial layer. As can be seen, using a very fine mesh with 20 elements between each layer produces results almost equivalent to using 3 elements. This is expected as the layers are very refined when compared to the width of the plate, making the mesh very fine even when using 1 element as the thickness of the layer. Thus,

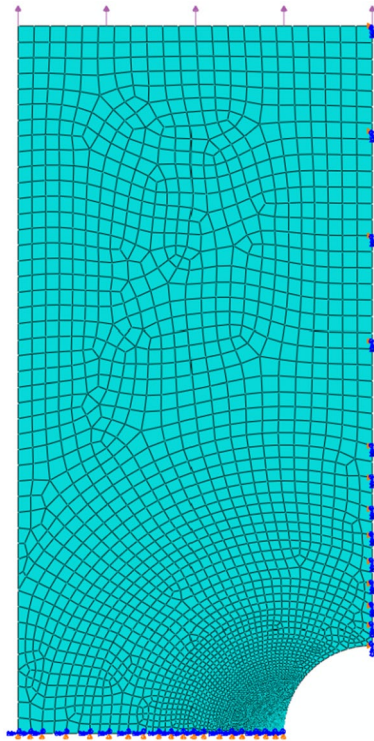


Fig. 3 Quarter symmetry mesh model for plate with hole diameter 0.25 the plate width



Fig. 4 Radial layers emanating from crack opening

using a layer thickness of at least 3 elements ensured that the mesh converged. The FEA model was validated by comparing the stress concentration factor of the model to the expected stress concentration from the literature.

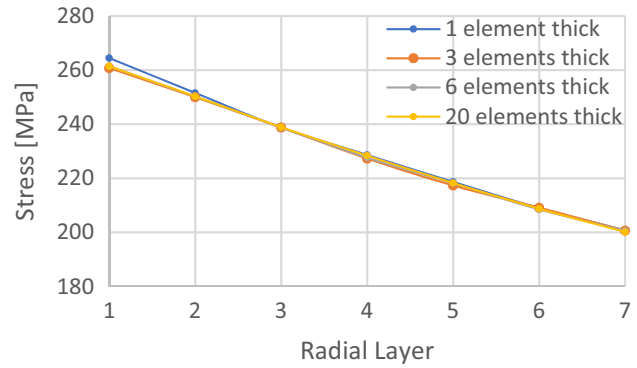


Fig. 5 Mesh sensitivity analysis

The stress concentration factor of the FEA model was calculated from the following equation:

$$K_t = \frac{\sigma_{max}}{\sigma_{nom}} \tag{5}$$

where the nominal stress is calculated by:

$$\sigma_{nom} = \frac{Load}{(plate_w - notch_d) thickness} \tag{6}$$

where $plate_w$ is the width of the plate and $notch_d$ is the diameter of the notch. The load is calculated by:

$$Load = 2wt \times 100 \text{ MPa} \tag{7}$$

And assuming that w is half the length of the plate, the equation for nominal stress simplifies to:

$$\sigma_{nom} = \frac{2wt \times 100 \text{ MPa}}{(2w - \frac{1}{2}w)t} = 133.33 \text{ MPa} \tag{8}$$

The max stress in the model was 323.51 MPa. Substituting values for max and nominal stress into Eq. 5 yields a stress concentration factor of 2.426. For a plate with a notch diameter 0.25 the width of the plate, Dowling [32] predicts a stress concentration factor of approximately 2.42, showing good correlation when compared to the FEA model. Thus, the FEA results can be trusted because the stress concentration factor expected from the literature shows strong correlation to the stress concentration factor produced by the FEA model. Figure 6 shows the stress gradient for the principal stress, σ_y , and the radial layers created around the crack opening.

Using the stress at the centroid of the elements within each layer, the average stress of every layer was determined. The resulting 1-D stress curve was fit with a 6th order polynomial curve to account for the biased spacing of the layers. A 6th order polynomial line was found to model the 1-D stress curve the best as opposed to a 3rd,

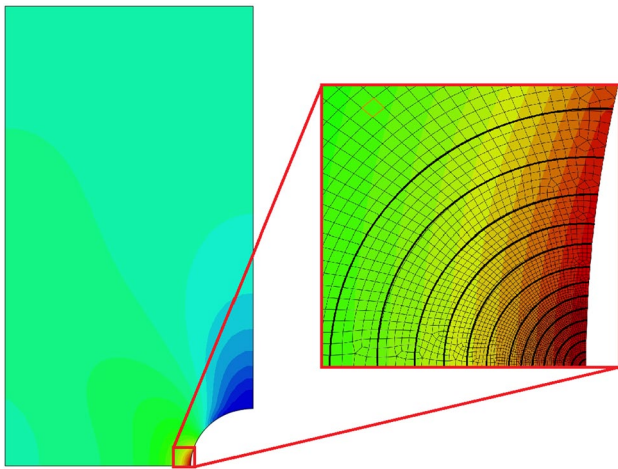


Fig. 6 σ_y stress gradient and radial layering around crack opening

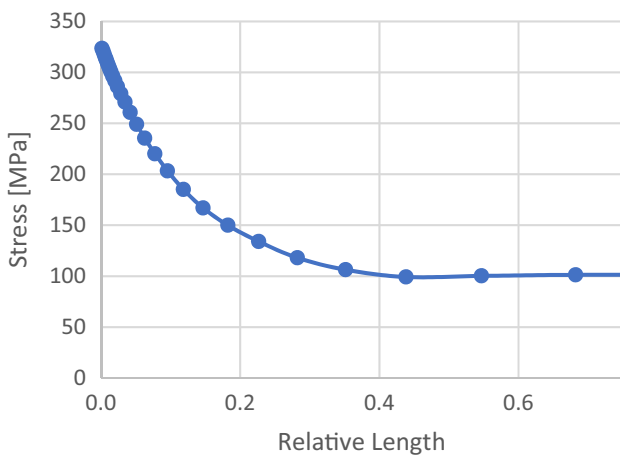


Fig. 7 Curve fit of stress profile

4th or any other order polynomial. The best fit curve can be seen superimposed over the discrete data in Fig. 7.

The fit line was then linearized for LRs of 1x, 2x, 3x, 5x, and 7x the length of the crack. Figure 8 shows the 1-D stress profile created from the average stress in each layer, as well as the linearized sections of the curve for a crack length 0.15 the width of the plate.

After the stress profile was linearized, the membrane and bending stresses for each LR were determined. Stress intensity factors for both the membrane component and the bending component were then calculated using Eqs. 2 and 3 and summed together to compute the total stress intensity factor for the component.

Stress intensity factors for various crack sizes ranging from 0.01 to 0.25 the width of the plate were computed in this way and compared to the handbook solutions given by Tada et al. [33]. This was repeated for a notch size of 0.5 the plate width, with errors for both hole diameters

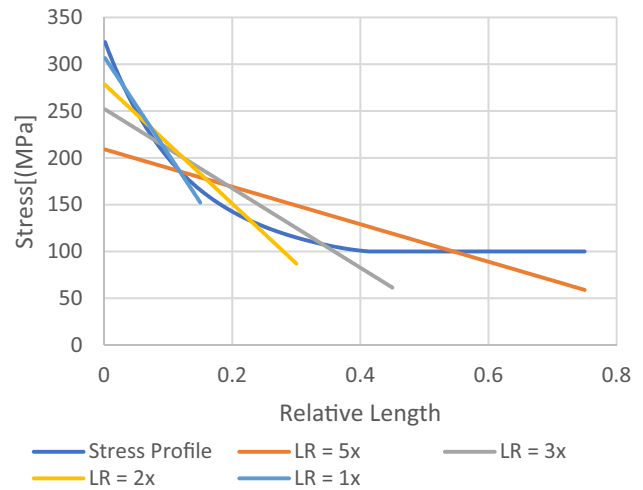


Fig. 8 1D average stress profile and linearized curves for plate with hole diameter 0.25 the plate width

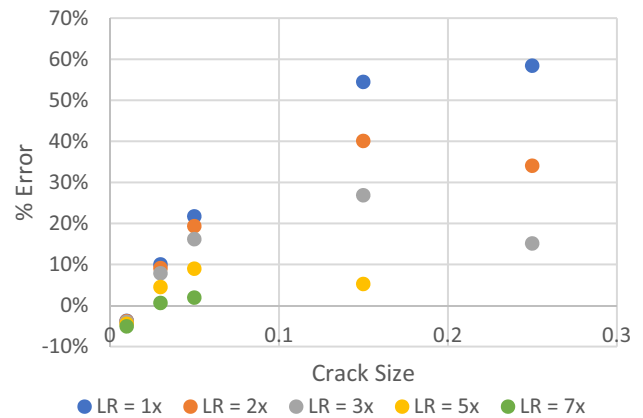


Fig. 9 Error in stress intensity factors for plate with hole diameter 0.25 the plate width

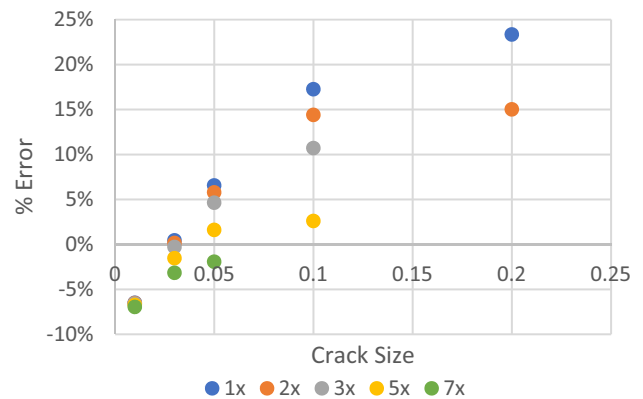


Fig. 10 Error in stress intensity factors for plate with hole diameter 0.5 the plate width

Table 1 7× LR stress intensity factors and errors for hole diameter 0.25 width of the plate

Defect size	K	K, Tada [33]	Error (%)
0.01	15.99	16.85	− 5.10
0.03	25.64	25.48	0.62
0.05	30.15	29.59	1.91

Table 2 7× LR stress intensity factors and errors for hole diameter 0.5 width of the plate

Defect Size	K	K, Tada [33]	Error (%)
0.01	21.74	23.37	− 6.97
0.03	36.45	37.65	− 3.18
0.05	44.85	45.73	− 1.94

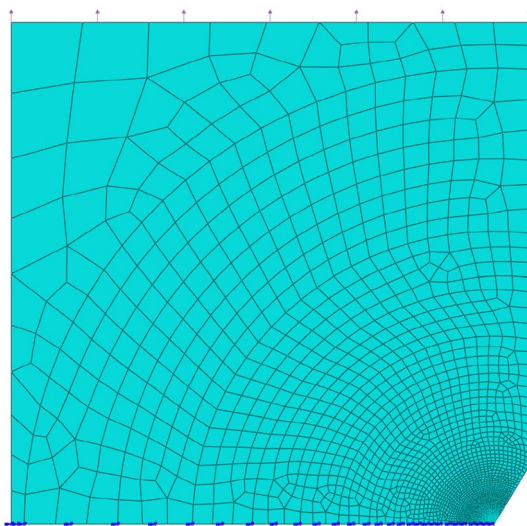


Fig. 11 Half symmetry mesh model for plate with 120-degree v-notch

displayed in Fig. 9 and 10. Tables 1 and 2 show the computed 7× LR stress intensity factors for various defect sizes. Notch sizes of 0.25 and 0.5 the width were chosen to compare to the handbook solutions more easily. Errors in both cases are seen to be minimized for a LR of 7×, ranging from −5.10 to 1.91% and −6.97 to −1.94%, respectively.

4.2 A crack emanating from a v-notched plate under tension

Flat plates with v-notches of 60° and 120° were also investigated. A 100 MPa pressure was uniformly applied to the top edge of the half symmetry model shown in Fig. 11. Symmetrical boundary conditions were applied such

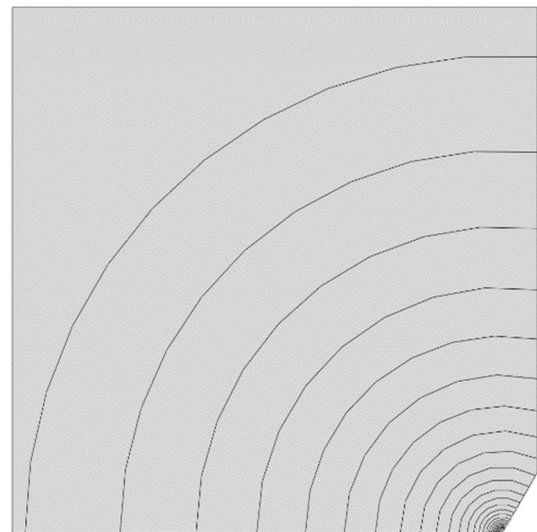


Fig. 12 Radial layers emanating from crack tip for plate with 120-degree v-notch

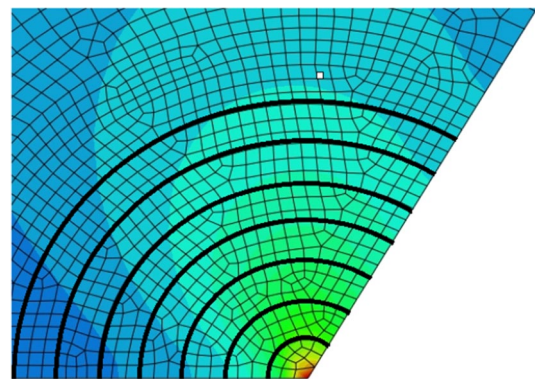


Fig. 13 The σ_y stress gradient and radial layering around crack opening

that the nodes on the bottom edge of the model have their displacement components normal to the horizontal plane constrained. Figure 12 shows the radial layers created around the crack opening and Fig. 13 displays the σ_y stress gradient and radial layers around the crack opening. Figure 14 shows the 1-D stress profile created from the average stress in each layer.

The same process used in case 4.1 was employed to determine the stress intensity factors for the v-notched plates. Figure 15 shows the error in the stress intensity factors for the 120-degree v-notch, displaying errors of −7.44% to 3.00% for a LR of 7× when compared to the closed form solution from Hasebe [34]. Figure 16 shows the error for the 60-degree v-notch, varying from −10.03 to 8.24% for a LR of 5×. Tables 3 and 4 display the computed 7× LR stress intensity factors for the 120-degree case and

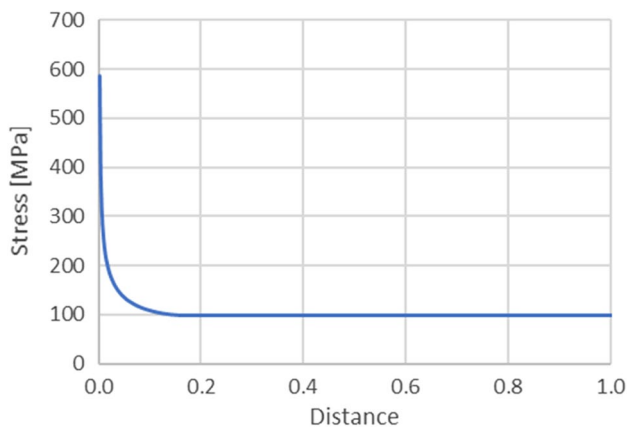


Fig. 14 1-D stress profile for plate with 120-degree v-notch

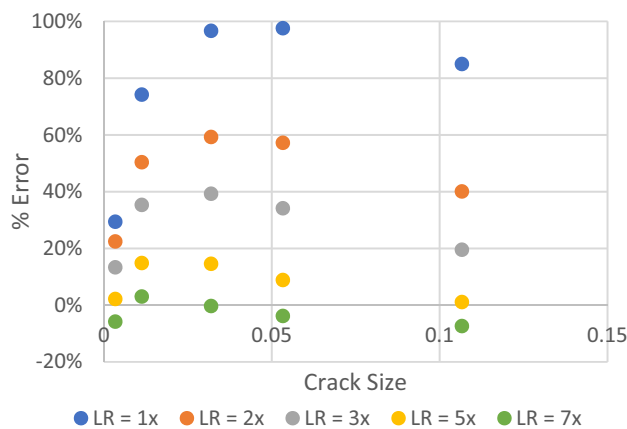


Fig. 15 Error in stress intensity factors for plate with 120-degree v-notch

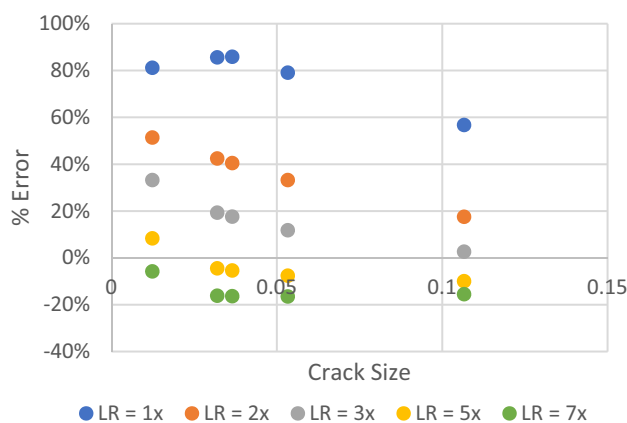


Fig. 16 Error in stress intensity factors for plate with 60-degree v-notch

the 5× LR stress intensity factors for the 60-degree case. The 7× LR for the 60-degree v-notch showed greater

Table 3 7× LR stress intensity factors and errors 120-degree v-notch

Defect size	K	K, Hasebe [34]	Error (%)
0.003	11.90	12.65	-5.90
0.032	15.06	14.63	3.00
0.032	17.04	17.10	-0.36
0.053	18.12	18.86	-3.89
0.107	20.98	22.66	-7.44%

Table 4 5× LR stress intensity factors and errors for 60-degree v-notch

Defect Size	K	K, Hasebe [34]	Error (%)
0.012	15.83	14.63	8.24
0.032	16.32	17.10	-4.57
0.037	16.53	17.49	-5.46
0.053	17.41	18.86	-7.67
0.107	20.39	22.66	-10.03

Table 5 Pressure vessel case configurations

Configuration	1	2	3
P (MPa)	6	6	6
ri (mm)	14	30	36
ro (mm)	40	40	40
t (mm)	26	10	4
ri/ro	0.35	0.75	0.9

error than the 5× LR. The steeper stress gradient of the 60-degree case shows that a lesser LR should be used since the stress profile reaches a constant value in a shorter distance as compared to the 120-degree case.

4.3 Cylindrical pressure vessel with an external crack

The pressurized cylinder investigated has an external longitudinal crack on the outer surface. A closed-form stress solution from Dowling [32] was used to determine the 1-D stress profile:

$$\sigma_t = \frac{pr_1^2}{r_2^2 - r_1^2} \left(\frac{r_2^2}{R^2} + 1 \right), \tag{9}$$

where p is the pressure, r₁ is the inner radii, r₂ is the outer radii, and R is the radius at any point. Three different configurations shown in Table 5 were studied, varying the inner and outer radii of the cylinder for each case. Using the process described in case 4.1, stress intensity factors were determined for each case. The results were compared

Table 6 2x LR stress intensity factors and errors for pressure vessel configuration 1

Defect Size	K	K, Budynas [35]	Error (%)
0.1	0.16	0.17	-5.04
0.2	0.25	0.26	-4.39
0.3	0.34	0.35	-2.24
0.4	0.44	0.44	0.97

Table 7 2x LR stress intensity factors and errors for pressure vessel configuration 2

Defect Size	K	K, Budynas [35]	Error (%)
0.1	0.89	0.99	-10.77
0.2	1.29	1.54	-16.30
0.3	1.63	2.14	-24.06
0.4	1.94	2.89	-32.92

Table 8 2x LR stress intensity factors and errors for pressure vessel configuration 3

Defect Size	K	K, Budynas [35]	Error (%)
0.1	1.83	2.18	-15.82
0.2	2.62	3.44	-23.83
0.3	3.24	4.90	-33.87
0.4	3.78	6.89	-45.11

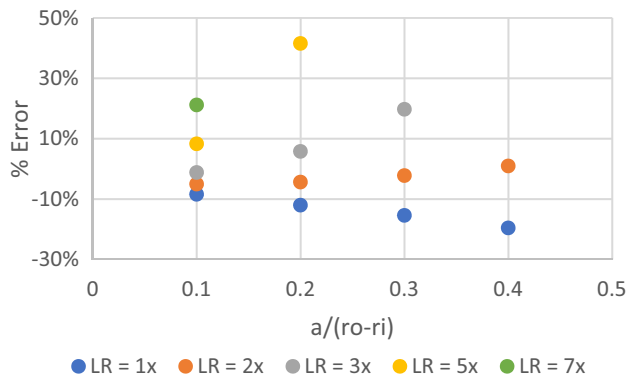


Fig. 17 Error in stress intensity factors for pressure vessel configuration 1

to solutions given by Budynas [35]. The error results for each case are shown in Tables 6, 7 and 8 and Figs. 17, 18 and 19. Configuration 1 produced errors ranging from -5.04 to 0.97% for a LR of 2x. For configurations 2 and 3 where the thickness of the cylinder is smaller compared to the outer radius, the 2x LR errors were much higher, ranging from -10.77 to -45.11%.

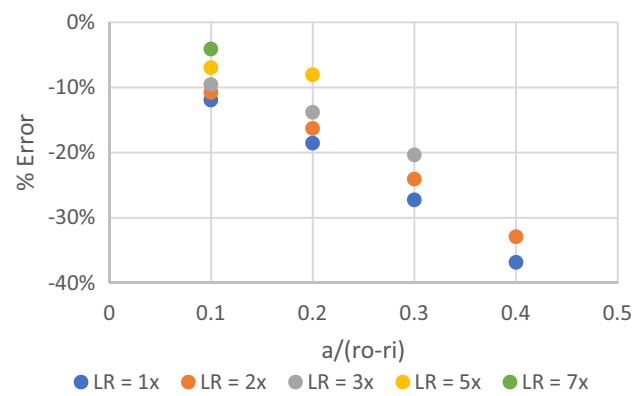


Fig. 18 Error in stress intensity factors for pressure vessel configuration 2

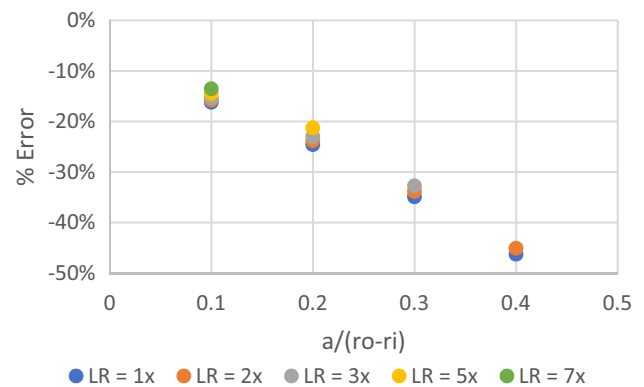


Fig. 19 Error in stress intensity factors for pressure vessel configuration 3

5 Observations and conclusions

The method proved to be effective for center hole plates, v-notched plates, and thick pressure vessels, generating values within 10% error for many different relative crack lengths. For center hole plates a larger LR of 5x or 7x showed results within 10% error when compared to handbook solutions. Inaccurate results for the LRs less than 5x demonstrate that not enough of the area around the crack is considered to properly capture the stress gradient affected zone around the crack. For larger crack lengths of more than 0.1 the length of the plate, a LR of 5x or 7x can exceed the bounds of the plate, and so the largest LR within the domain of the plate should be used. When considering v-notched plates, a LR of 5x proved to be best for a 60-degree v-notch and a LR of 7x was best for a 120-degree v-notch.

For the thick pressure vessel in configuration 1, a LR of 2x gave the least error, unlike the other cases where a larger LR of 5x or 7x produced the best results. This is

because the stress field moving away from the crack shows an increase in stress. There is no far field stress region in this case where the stress would reach some constant value, as opposed to the cases of the center hole and v-notch plates.

For pressure vessel configurations 2 and 3 where wall thickness was thinner, the method produced larger errors in stress intensity factors. For these configurations the stress gradient is small, and therefore the stress profile is essentially constant. As a result, there is no need to employ a numerical scheme to predict the stress intensity for this simple, zero stress gradient case.

Previous work done by Abou-Hanna [31] is closely related to this work; it employs the radial layering technique and requires the use of a distance-based complex weighting scheme and computation of the relative stress gradient which resulted in higher errors in some cases treated in this study. The current method does not require such complex computations and is simpler while also maintaining results within $\pm 10\%$ for all cases.

The technique showed the best success when using larger LR of $5\times$ or $7\times$ when the area around the crack has a larger stress gradient and using a smaller LR of $2\times$ when the stress gradient around the crack is smaller. This shows that when the crack is in an area of high stress gradient, more area around the crack is required to accurately determine stress intensity factor.

Since the technique can be employed for a 2-D FEA model, the computation time is very short. Practical use of this technique would likely require implementation of an automated method of calculating the average stresses within each layer. Implementing this method for a 3-D FEA would be a logical next step in exploring the prospects of this technique.

Author contributions All authors contributed to the study, conception, and design. Material preparation, data collection and analysis were performed by BS and JA-H. The first draft of the manuscript was written by BStorm and all authors commented on previous versions of the manuscript. All authors read and approved the final manuscript.

Funding The authors declare that no funds, grants, or other support were received during the preparation of this manuscript.

Data availability All datasets generated during and/or analyzed during the current study are available from the corresponding author on reasonable request.

Declarations

Conflict of interest On behalf of all authors, the corresponding author states that there is no conflict of interest.

Open Access This article is licensed under a Creative Commons Attribution 4.0 International License, which permits use, sharing, adaptation, distribution and reproduction in any medium or format, as long as you give appropriate credit to the original author(s) and the source, provide a link to the Creative Commons licence, and indicate if changes were made. The images or other third party material in this article are included in the article's Creative Commons licence, unless indicated otherwise in a credit line to the material. If material is not included in the article's Creative Commons licence and your intended use is not permitted by statutory regulation or exceeds the permitted use, you will need to obtain permission directly from the copyright holder. To view a copy of this licence, visit <http://creativecommons.org/licenses/by/4.0/>.

References

1. Irwin GR (1957) Analysis of stresses near the end of a crack traversing a plate. *J Appl Mech* 24:361. <https://doi.org/10.1115/1.4011547>
2. Murakami Y (2001) Stress intensity factors handbook, vol 4. Society of Materials Science, Japan
3. Murakami Y (2002) Metal fatigue: effects of small defects and nonmetallic inclusions. Elsevier, Oxford
4. Murakami Y, Endo M (1983) Quantitative evaluation of fatigue strength of metals containing various small defects or cracks. *Eng Fract Mech* 17:1–15. [https://doi.org/10.1016/0013-7944\(83\)90018-8](https://doi.org/10.1016/0013-7944(83)90018-8)
5. Murakami Y, Endo M (1986) Effects of hardness and crack geometries on ΔK_{th} of small cracks emanating from small defects. In: Miller KJ, de los Rios ER (eds) The behavior of short fatigue cracks. Mechanical Engineering Publication, London, pp 275–293
6. Glinka G (1985) Calculation of inelastic notch-tip strain-stress histories under cyclic loading. *Eng Fract Mech* 22(5):839–854. [https://doi.org/10.1016/0013-7944\(85\)90112-2](https://doi.org/10.1016/0013-7944(85)90112-2)
7. Bloom J, Van Der Sluys WA (1977) Determination of the stress intensity factor for gradient stress fields. *J Press Vessel Technol* 99(3):477–484. <https://doi.org/10.1115/1.3454562>
8. Chen DH (1994) Stress intensity factors for V-notched strip under tension or in-plane bending. *Int J Fract* 70:81–97. <https://doi.org/10.1007/BF00018137>
9. Liu Y et al (2008) Numerical methods for determination of stress intensity factors of singular stress field. *Eng Fract Mech* 75:4793–4803. <https://doi.org/10.1016/j.engfracmech.2008.06.007>
10. Chell G (1975) The stress intensity factors for centre and edge cracked sheets subject to an arbitrary loading. *Eng Fract Mech* 7:137. [https://doi.org/10.1016/0013-7944\(75\)90070-3](https://doi.org/10.1016/0013-7944(75)90070-3)
11. Chell G (1976) The stress intensity factors for part through thickness embedded and surface flaws subject to a stress gradient. *Eng Fract Mech* 8:331–340. [https://doi.org/10.1016/0013-7944\(76\)90013-8](https://doi.org/10.1016/0013-7944(76)90013-8)
12. Bueckner H (1997) A novel principal for the computing of stress intensity factors. *Z Angew Math Mech* 50:529–545
13. Rice J (1972) Some remarks on elastic crack-tip stress field. *Int J Solids Struct* 8:751–758. [https://doi.org/10.1016/0020-7683\(72\)90040-6](https://doi.org/10.1016/0020-7683(72)90040-6)
14. Ju S, Chung H (2007) Accuracy and limit of a least-squares method to calculate 3D notch SIFs. *Int J Fract* 148:169–183. <https://doi.org/10.1007/s10704-008-9193-7>
15. Xu J et al (1999) Numerical methods for the determination of multiple stress singularities and related stress intensity coefficients. *Eng Fract Mech* 63:775–790. [https://doi.org/10.1016/S0013-7944\(99\)00044-2](https://doi.org/10.1016/S0013-7944(99)00044-2)

16. Courtin S et al (2005) Advantages of the J-integral approach for calculating stress intensity factors when using the commercial finite element software ABAQUS. *Eng Fract Mech*. <https://doi.org/10.1016/j.engfracmech.2005.02.003>
17. Rice J (1968) A path independent integral and the approximate analysis of strain concentration by notches and cracks. *J Appl Mech* 35(2):379–386. <https://doi.org/10.1115/1.3601206>
18. Gopichand A et al (2012) Computation of stress intensity factor of brass plate with edge crack using J-integral technique. *Int J Res Eng Technol* 1(3):261–266
19. Nikolova G, Yanakieva A (2017) Determination of the SIF and ERR in a cracked bi-material elements using FEM, LEFM energy approach and analytical calculations. In: 13th National congress on theoretical and applied mechanics
20. Azmi M et al (2017) On the ΔJ -integral to characterize elastic-plastic fatigue crack growth. *Eng Fract Mech*. <https://doi.org/10.1016/j.engfracmech.2017.03.041>
21. Han Q et al (2015) Determination of stress intensity factor for mode I fatigue crack based on finite element analysis. *Eng Fract Mech*. <https://doi.org/10.1016/j.engfracmech.2015.02.019>
22. Alatawi I, Trevelyan J (2015) A direct evaluation of stress intensity factors using the extended dual boundary element method. *Eng Anal Bound Elem* 52:56–63. <https://doi.org/10.1016/j.enganabound.2014.11.022>
23. Gupta P et al (2017) Accuracy and robustness of stress intensity factor extraction methods for the generalized/eXtended finite element method. *Eng Fract Mech* 179:120–153. <https://doi.org/10.1016/j.engfracmech.2017.03.035>
24. Farahani B et al (2017) Stress intensity factor calculation through thermoelastic stress analysis, finite element and RPIM meshless method. *Eng Fract Mech* 183:66–78. <https://doi.org/10.1016/j.engfracmech.2017.04.027>
25. Roux S, Hild F (2006) Stress intensity factor measurements from digital image correlation: post-processing and integrated approaches. *Int J Fract* 140:141–157. <https://doi.org/10.1007/s10704-006-6631-2>
26. Gonzales G et al (2017) A J-integral approach using digital image correlation for evaluating stress intensity factors in fatigue cracks with closure effects. *Theoret Appl Fract Mech* 90:14–21. <https://doi.org/10.1016/j.tafmec.2017.02.008>
27. Tavares P et al (2015) SIF determination with digital image correlation. *Int J Struct Integrity* 6:668–676
28. Berto F et al (2017) Some methods for rapid evaluation of the mixed mode NSIFs. *Procedia Struct Integrity* 3:126–134. <https://doi.org/10.1016/j.prostr.2017.04.022>
29. Dong Y, Guedes Soares C (2019) Stress distribution and fatigue crack propagation analyses in welded joints. *Fatigue Fract Eng Mater Struct* 42:69–83. <https://doi.org/10.1111/ffe.12871>
30. McKinley T (2013) A reduced complexity method for stress-intensity factor determination using stress gradients. Master's thesis, Bradley University, ProQuest Dissertations Publishing, Peoria
31. Abou-Hanna J (2020) Simplified stress gradient method for stress-intensity factor determination. *Int J Mech Mechatron Eng*. <https://doi.org/10.6084/m9.figshare.12489788>
32. Dowling N (2013) Mechanical behavior of materials: engineering methods for determination, fracture, and fatigue. Pearson, Harlow
33. Tada H, Paris P, Irwin G (2000) The stress analysis of cracks handbook, 3rd edn. ASME, New York
34. Hasebe N, Iida J (1978) A crack originating from a triangular notch on a rim of a semi-infinite plate. *Eng Fract Mech* 10:773–782. [https://doi.org/10.1016/0013-7944\(78\)90032-2](https://doi.org/10.1016/0013-7944(78)90032-2)
35. Budynas R, Nisbeth J (2011) Shigley's mechanical engineering design. McGraw-Hill, New York

Publisher's Note Springer Nature remains neutral with regard to jurisdictional claims in published maps and institutional affiliations.